DEUTSCHES ELEKTRONEN-SYNCHROTRON
INSTITUT FÜR HOCHENERGIEPHYSIK

DESY 94-091
June 1994

The $b\bar{b}$ -Pair Production and the Higgs Signal in the Reaction $e^+e^- \to e^+e^-b\bar{b}$ at LEPII and NLC Energies

E. Boos

Deutsches Elektronen-Synchrotron DESY
Institut für Hochenergiephysik IfH, Zeuthen
and
Nuclear Physics Institute, Moscow State University, Russia

M. Sachwitz, H. J. Schreiber

Deutsches Elektronen-Synchrotron DESY
Institut für Hochenergiephysik IfH, Zeuthen

S. Shichanin

Deutsches Elektronen-Synchrotron DESY
Institut für Hochenergiephysik IfH, Zeuthen
and
Institute for High Energy Physics, Protvino, Moscow Region, Russia

ISSN 0418-9833

PLATANENALLEE 6 - 15738 ZEUTHEN

To be sure that your preprints are promptly included in the
HIGH ENERGY PHYSICS INDEX,
send them to (if possible by air mail):

DESY **Bibliothek** **Notkestraße 85** **22603 Hamburg** **Germany**	**DESY-IfH** **Bibliothek** **Platanenallee 6** **15738 Zeuthen** **Germany**

DESY 94- 091
June 1994

ISSN 0418-9833

The $b\bar{b}$-pair Production and the Higgs Signal in the Reaction $e^+e^- \longrightarrow e^+e^- b\bar{b}$ at LEPII and NLC Energies

E. Boos[1,2], M. Sachwitz[1], H. J. Schreiber[1] and S. Shichanin[1,3]

[1]DESY-Institut für Hochenergiephysik, Zeuthen, FRG
[2]Nuclear Physics Institute, Moscow State University, 119899, Moscow, Russia
[3]Institute for High Energy Physics, 142284, Protvino, Moscow Region, Russia

Abstract

Results of calculations of all tree-level Standard Model diagrams for the reaction $e^+e^- \longrightarrow e^+e^- b\bar{b}$ in the energy range of LEPII and the Next e^+e^- Linear Collider are presented. The complete matrix element was calculated by means of the software package CompHEP; phase space integration and event generation were carried out with the computer programs BASES/SPRING with additional regularizations necessary in order to handle singularities. The contributions of the dominating subsets of diagrams, the possible interference terms and their influence on the Higgs signal are studied in detail. Agreement with results of previous calculations as well as with those derived from simple analytical approximations is demonstrated. Encouraging results were obtained regarding the extraction of the Higgs signal from the overwhelming background.

1 Introduction

Reactions like $e^+e^- \longrightarrow 2$ leptons $+ b\bar{b}$ provide the most promising framework for light and intermediate ($M_H \lesssim 140$ GeV) Higgs searches within the Standard Model [1] at LEPII and Next e^+e^- Linear Collider (NLC) energies (see e.g. refs. [2, 3, 4, 5]). They provide the channels for detailed investigations of the Higgs sector since the properties expected for the Higgs may be extracted which great confidence from such 4-body final states. Since the Higgs is produced either in the Higgsstrahlung reaction

$$e^+e^- \longrightarrow H^0 Z \tag{1}$$

with the subsequent decay $H^0 \to b\bar{b}$ and $Z \to l\bar{l}$ ($l = e, \mu, \tau, \nu_e, \nu_\mu, \nu_\tau$) or in the fusion process

$$e^+e^- \longrightarrow l\bar{l}H^0 \tag{2}$$

with $l = e$ or ν_e and subsequent $H^0 \to b\bar{b}$ decay, the framework for Higgs detection and determination of its properties is the final state $l\bar{l}\,b\bar{b}$. It seems therefore mandatory to investigate this final state in detail and to extract the Higgs signal from it, taking into account all competing subprocesses and possible interferences which lead to the same $l\bar{l}\,b\bar{b}$ final state. Such a procedure is further supported by the expectation that the background is much larger than the Higgs signal itself, and a simultanous investigation of both components leads to more appropriate background substracted Higgs studies.

In recent papers detailed analyses have been carried out for the reaction [6, 7]

$$e^+e^- \longrightarrow \mu^+\mu^- b\bar{b} \tag{3}$$

as well as for [8, 9]

$$e^+e^- \longrightarrow \nu\bar{\nu}b\bar{b}. \tag{4}$$

In order to complete the analysis of the 2 leptons + $b\bar{b}$ final state configuration we present in this paper our results for the reaction

$$e^+e^- \longrightarrow e^+e^- b\bar{b}. \tag{5}$$

Reaction (5) provides not only a promising signature for the Higgs boson, it also represents in cases of undetected outgoing electrons a serious background to the Higgs signal in reaction (4). Furthermore, the calculation of the total $b\bar{b}$ pair production rate in reaction (5) is important for top quark physics and for estimating the background in searches for possible new physics at higher energies.

Compared to processes (3) and (4) the reaction $e^+e^- \longrightarrow e^+e^- b\bar{b}$ possesses the greatest complexity. It involves the largest number of possible lowest order diagrams and in addition it contains a number of singularities in phase space which have to be carefully taken into account. Most of these singularities are connected with final state electrons produced in the very forward direction. In our calculations we use the computer program CompHEP[10] to generate all possible Standard Model tree-level diagrams and the package BASES/SPRING [11] for integration over phase space. In the past several Monte Carlo generators for 4-fermion final states in e^+e^- collisions have been created [12, 13, 14], but none of them takes into account all contributing diagrams and their possible interferences. As an example, one of the recently developed generators, FERMISV [15], includes all lowest order diagrams with photon and Z boson propagators in reaction (5) but omits the Higgs boson intermediate states.

This paper is organized as follows. In sect. 2 we present and discuss all contributing diagrams. The total cross section for reaction (5) is calculated as a function of the center of mass (cms) energy $\sqrt{s}$ and compared with the expected Higgs rate. Sect. 3 is devoted to a detailed study of Higgs production. In particular, its cross section as a function of $\sqrt{s}$and the H^0 mass are presented and the two Higgs production mechanisms and their interferences are discussed. In sect. 4 the cross sections of various subsets of background diagrams which contribute to different kinematical regions are presented and compared with simple semi-analytical results using the formulas summarized in the Appendix.

Sect. 5 contains a summary of the strengths of the interference terms between the subsets of diagrams discussed, and based on that, our suggestion for an approximate description of reaction (5) at LEPII energies as well as around $\sqrt{s} = 500$ GeV. In sec. 6 it will be demonstrated that by application of simple cuts the H^0 signal can be clearly extracted from the overwhelming background. The summary and concluding remarks are presented in sect. 7.

In all cases when event numbers are presented or discussed, they are normalized to an integrated luminosity of $\mathcal{L} = 500$ pb^{-1} or $\mathcal{L} = 10$ fb^{-1} at $\sqrt{s} =$ 200 GeV and 500 GeV, respectively,

2 The cross section of the reaction $e^+e^- \longrightarrow e^+e^- b\bar{b}$

The calculation of the cross section for reaction (5) has been performed in the same manner as for reactions (3) and (4) in refs. [7, 8]. This procedure has also been used recently in an estimation of single top quark production in the LEPII energy range [16].

The main steps in our calculation are the following. The generation of Feynman diagrams, the analytical expressions for the matrix elements squared and the corresponding optimized FORTRAN codes have been obtained by means of the computer package CompHEP. The integration over phase space, after smoothing of singular variables in order to improve the efficiency of the program, and the event generation have been done by employing the Monte Carlo integrator and event generation system BASES/SPRING. We would like to point out that in contrast to previous calculations [7, 8, 16], it was necessary to employ a quadruple precision in the computer code. The calculation of the diagrams includes a non-zero mass value of the electron and Breit-Wigner distributions for the Higgs and Z bosons in the intermediate states. The results presented were obtained taking into account the Standard Model parameters and the tree-level Higgs width. For the coupling factor α we used the Thomson limit 1/137 in cases of long distance physics, i.e. in cases of soft photon exchanges, and otherwise 1/128 [17]. The calculations were carried out in the t'Hooft-Feynman gauge.

All lowest order diagrams contributing to reaction (5) are collected in Fig. 1. The two diagrams in the first row are responsible for the Higgs production either via the Higgsstrahlung process $e^+e^- \longrightarrow H^0Z$ or the ZZ fusion reaction $e^+e^- \longrightarrow e^+e^- H^0$. The Higgsstrahlung diagram is analogous to that in the reaction $e^+e^- \longrightarrow \mu^+\mu^- b\bar{b}$ (or $e^+e^- \longrightarrow \nu\bar{\nu}\, b\bar{b}$) with relative weights as determined by the $Z \to e^+e^-$, $\mu^+\mu^-$ and $\nu\bar{\nu}$ branching fractions. The ZZ fusion contribution is suppressed by about a factor of ten with respect to the

corresponding W^+W^- fusion process in the reaction $e^+e^- \longrightarrow \nu\bar{\nu}\, H^0$ due to the different couplings of the Z and W boson to leptons (see [4]).

The diagrams in the second raw in Fig. 1 are of multiperipheral nature and are governed by the 2-to-2 processes $\gamma^*(Z)\gamma^*(Z) \rightarrow b\bar{b}$.

Diagrams in the third and fourth row can be considered as due to $\gamma^*(Z)e^{\pm} \rightarrow \gamma^*(Z)e^{\pm}$ subprocesses which proceed either via electron (positron) t-channel exchanges or via s-channel production with subsequent radiation of a $\gamma^*(Z)$ from an off-shell electron (positron).

The fifth row of diagrams corresponds to the 2-to-2 subprocesses $e^+e^- \longrightarrow \gamma^*(Z)\gamma^*(Z)$ with subsequent decays of $\gamma^*(Z)$ to e^+e^- and $b\bar{b}$.

The diagrams in the last row of Fig. 1 correspond to γ^*/Z s-channel formation with $b\bar{b}$ or e^+e^- production and subsequent radiation of a photon/Z and its decay into e^+e^- or $b\bar{b}$.

We would like to point out that these five classes of subprocesses are to a good approximation gauge invariant by themselves, so that their individual cross sections can be calculated and compared with each other.

In Fig. 2 the total cross section for the reaction $e^+e^- \longrightarrow e^+e^-b\bar{b}$ is presented as a function of $\sqrt{s}$ between 200 GeV and 1 TeV. It is worth emphasizing that all diagrams of Fig. 1 and their interferences were taken into account to obtain these values. The cross section of reaction (5) does not strongly vary with $\sqrt{s}$; it increases by a factor of ~ 4 in the energy range considered. In addition, Fig. 2 shows also the total amount of H^0 production to the $e^+e^-\, b\bar{b}$ final state. The H^0 rate is however about two or more orders of magnitude lower. The figure indicates that the ratio of the H^0 to the total background rate turns out to be best in the LEPII energy range where the Higgsstrahlung mechanism dominates. However, also at this energy the background is overwhelming and efficient cuts have to be applied in order to reduce the background substantially without removing the few H^0 events expected. In order to optimize such cuts we study separately in more detail the behaviour of the signal and the different background contributions.

3 The Higgs boson signal

In Fig. 3a we present the total Higgs boson cross section in the reaction $e^+e^- \longrightarrow e^+e^-\, b\bar{b}$ for five Higgs masses between 80 GeV and 140 GeV as a function of the cms energy, in the range $\sqrt{s} = 160$ GeV to 500 GeV. The behaviour of these distributions is well understood. At low energies (around LEPII energies) the Higgsstrahlung cross section dominates, as seen in Fig. 3b. It rises sharply near threshold,reaches a maximum at $\sqrt{s} \sim M_Z + \sqrt{2}M_{H^0}$ and

falls down with 1/s at higher energies. The H^0 fusion mechanism (Fig. 3c), negligible at LEPII energies, rises continously with increasing energy ($\sim$ log s) and dominates around or above 500 GeV. However, comparing the absolute H^0 cross section in reaction (5) at 500 GeV with that in reaction (4), $e^+e^- \longrightarrow \nu\bar{\nu}\, b\bar{b}$ [8, 9], its value is about one order of magnitude lower due to the different couplings of Z and W to the Higgs and fermions (see [4, 18]). Fig. 3d shows the interference pattern between both production mechanisms. Although it is very small, it can be noticed that the larger the Higgs mass the smaller is the interference contribution.

Table 1 summarizes the number of H^0 events expected for an integrated luminosity of $\mathcal{L} = 500$ pb^{-1} and $\mathcal{L} = 10$ fb^{-1} at $\sqrt{s} = 200$ GeV and 500 GeV, respectively, for the five Higgs masses indicated in Fig. 2. As can be seen, the number of Higgs events expected at LEPII are either very small or completely negligible. Better possibilities for Higgs detection occur at energies around $\sqrt{s} = 500$ GeV. Higgs production above 500 GeV will not be discussed here, since the most appropriate energy range for Higgs detection is in between LEPII energies and 500 GeV, for Higgs masses considered in this paper (80 $\leq M_{H^0} \leq$ 140 GeV). Higgs bosons with masses larger than 140 GeV are best be searched for in the $ZZ^*(ZZ)$ or $WW^*(WW)$ decay modes rather than in the $H^0 \rightarrow b\bar{b}$ decay channel, so that the final states expected are different from 2 leptons + $b\bar{b}$ [18].

Some H^0 event distributions as expected at $\sqrt{s} = 200$ GeV are presented in Fig. 4, for $M_{H^0} = 80$ GeV and $\mathcal{L} = 500$ pb^{-1}. In particular, we present in this figure the cosine of the electron production angular distribution, cosΘ_e, the total $b\bar{b}$-quark energy distribution, $E_{b\bar{b}}$, the total $b\bar{b}$ transverse momentum distribution, $p_\perp^{b\bar{b}}$, and the e^+e^- invariant mass distribution, $M_{e^+e^-}$. Detailed inspection of the event distributions in these variables leads us to conclude that appropriate cuts should remove the overwhelming background to a very small or negligible level while keeping most of the signal. For further details we refer to sect. 6.

The analogous H^0 event distributions for $M_{H^0} = 140$ GeV and $\sqrt{s} = 500$ GeV are presented in Fig. 5, where different H^0 production mechanisms compete and the background exhibits a somewhat different behaviour than at $\sqrt{s} =$ 200 GeV (see the next sect. for more details).

4 The background contributions

Since the background in reaction (5) is about two orders of magnitude larger than the Higgs signal, it is important to investigate the different mechanisms

contributing to different phase space regions in detail so that reasonable cuts can be applied for their suppression while retaining the H^0 signal. According to the classification of the diagrams in Fig. 1 we discuss now their individual characteristics in turn.

4.1 The multiperiphal background contribution

We denote as *multiperipheral* background that part which proceeds via the multiperipheral diagrams in the second row of Fig. 1. Such contributions of massive fermion pair production in e^+e^- collisions have been studied in a number of papers and is known in QED for a long time; e.g. Landau and Lifshitz [19] calculated the main e^+e^- pair production cross section in 1934.

The dominant part of the multiperipheral background is expected to be due to photon-photon exchange with very small momentum transfer squared. This background has the asymptotic form [20]

$$\sigma \sim \frac{1}{m_f^2} ln^2 \frac{s}{m_e^2} ln \frac{s}{m_f^2}, \tag{6}$$

where the term $\ln^2(s/m_e^2)$ is related to the photon propagators and the term $\ln(s/m_f^2)$ is connected to the subprocess $\gamma^*\gamma^* \to f\bar{f}$.

A more accurate but still approximate analytical formula may be found in ref. [21], while a number of Monte-Carlo generators, proposed for this kind of multiperipheral diagrams, are discussed in [12, 13, 14, 15].

In order to gain confidence in our calculation of the multiperipheral background diagrams, we have first applied the formalism to the reaction $e^+e^- \longrightarrow e^+e^-\,\mu^+\mu^-$ for which detailed and accurate calculations exist [12]. Very good agreement between our results and those of ref. [12] has been found, so that the procedure applied for smoothing of singular variables, mandatory in order to obtain stable numerical results, is strongly supported. Fig. 6 shows cross section values obtained for the multiperipheral background in reaction (5) (full curve) as function of $\sqrt{s}$ and, for comparison, the results from a simple analytical formula, given in the Appendix, based on the $\gamma^*\gamma^* \to b\bar{b}$ two-body reaction convoluted with the appropriate photon spectrum from the electron (dashed curve). The agreement with our calculation, which involves all possible multiperipheral diagrams, is excellent. Hence, as expected, $\gamma^*\gamma^*$ exchanges represent the overwhelming contribution to the multiperipheral background. Multiperipheral γ^*Z and ZZ exchange diagrams are suppressed by about a factor of 10^{-3} and 10^{-6}, respectively. Interferences between the multiperipheral diagrams were found to be very small; they are at best of the order of the γ^*Z exchange contribution.

According to the cross sections obtained one expects a large number of $b\bar{b}$ events from the multiperipheral $\gamma^*\gamma^*$ mechanism, namely about 500 at $\sqrt{s} = 200$ GeV and about 30000 at $\sqrt{s} = 500$ GeV. Hence, this mechanism represents a large background to the H^0 signal. Variables which might be useful for background suppression while retaining the H^0 events have been searched for and some of them are presented in Fig. 7. The number of events shown are expected for an integrated luminosity of 500 pb^{-1} and 10 fb^{-1} at $\sqrt{s} = 200$ GeV and $\sqrt{s} = 500$ GeV, respectively.

4.2 The background from $\gamma^*/Ze \to \gamma^*/Ze$ contributions

The third and fourth row of the diagrams in Fig. 1 (denoted as *single cascade* diagrams) involve the subreaction $\gamma^*/Ze \to \gamma^*/Ze$ which proceeds either via electron t-channel exchanges or s-channel off-shell electron production with subsequent radiation of a photon or Z boson. The calculation of all diagrams contributing to this part of the background and their interferences results in cross sections also presented in Fig. 6 as function of $\sqrt{s}$. In addition, we have also carried out cross section estimations for this background part using a simple semi-analytical approach as given in the Appendix (dashed curve in Fig. 6). As can be seen, satisfactory agreement between the complete calculation and the approximative scheme occurs. Since the total rate of this background is also substantial a search for sensible variables is needed in order to suppress most of the background in Higgs search analyses. The variables selected are presented in Fig. 8 for $\sqrt{s}$ = 200 GeV and 500 GeV, assuming for the event number estimation an integrated luminisity of 500 pb^{-1} and 10 fb^{-1}, respectively.

4.3 The background from $e^+e^- \longrightarrow \gamma^*(Z)\gamma^*(Z)$ contribution

The *double cascade* diagrams of the fifth row in Fig.1 correspond to the 2-to-2 body processes $e^+e^- \longrightarrow \gamma^*(Z)\gamma^*(Z)$ with subsequent decays of $\gamma^* \to e^+e^-\,(b\bar{b}\,)$ and $Z \to b\bar{b}\,(e^+e^-\,)$. The total cross sections associated with this type of background are also shown as function of $\sqrt{s}$ in Fig. 6 (full curve). In addition, we also present the cross sections expected for the four separate contributions, $e^+e^- \longrightarrow \gamma^*\gamma^*$, $e^+e^- \longrightarrow \gamma^*Z \to (e^+e^-\,)(b\bar{b}\,)$, $e^+e^- \longrightarrow \gamma^*Z \to (e^+e^-\,)(b\bar{b}\,)$ and $e^+e^- \longrightarrow ZZ$, including possible interference terms. As can be seen, the γ^*Z final state with $\gamma^* \to e^+e^-$ and $Z \to b\bar{b}$ decays represents the bulk of this background. Double Z production is smaller by about a factor of 10 (5) at 200 (1000) GeV and comparable to the Higgs production rate in the LEPII energy range. Results from some simple semi-analytical calculations

which are outlined in the Appendix, are also shown in Fig. 6 as dashed curves. The agreement between the complete and approximate schemes is reasonable.

Fig. 9 show relevant event distributions for this background in variables selected for background suppression, again normalized to an integrated luminosity of 500 pb^{-1} and 10 fb^{-1} at $\sqrt{s}$ = 200 GeV and 500 GeV, respectively.

For completeness we have also calculated the cross sections for the remaining s-channel diagrams shown in the last row of Fig.1, including possible interferences. This background is found to be very small and would amount to less than one event at 200 GeV (for $\mathcal{L}$ = 500 pb^{-1}) and to about three events at 500 GeV ($\mathcal{L}$ = 10 fb^{-1}). Hence, we omit these diagrams and their interfereces in our further discussion.

5 Study of interferences and a suggestion for an approximative description of the reaction $e^+e^- \longrightarrow e^+e^- b\bar{b}$

In previous sections we have studied the contributions of the Higgs signal and the different background subsets separately, including only the interferences between the diagrams for each subset. In this part we will search for possible interferences between the different subsets themselves, and according to the results found we suggest an approximation scheme to describe reaction (5) reasonably well over a very large range in $\sqrt{s}$.

At first, it turns out that the interferences between the Higgs diagrams and all the background diagrams are very small. Typically, their contributions are in the range 10^{-4} - 10^{-5} fb and the largest interference contribution of 10^{-3} fb occurs with the multiperipheral diagrams (second row in Fig. 1) at $\sqrt{s} = 200$ GeV. Such a behaviour is not surprising since Higgs production and most of the background mechanisms contribute to very different phase space regions, and also because of the different spins of the H^0 and the Z boson and photon. Therefore, interferences between the Higgs boson and the background can with confidence be neglected in any further studies.

Furthermore, we have searched systematically for interferences between the several background subsets as indicated in Fig. 1. The result is that only interferences between the single cascade diagrams with $Z \to b\bar{b}$ decay and the double cascade diagrams wirh $\gamma^* \to e^+e^-$ and $Z \to b\bar{b}$ decays turn out to be significant: -24 fb at $\sqrt{s} = 200$ GeV, -7.8 fb at $\sqrt{s} = 500$ GeV and -4.0 fb at $\sqrt{s} = 1$ TeV. Interferences between the single cascade diagrams with $\gamma^* \to b\bar{b}$ and $Z \to b\bar{b}$ decays themselves are found to be -3.2 fb, -4.3 fb and -4.9 fb at $\sqrt{s} = 200$, 500 GeV and 1 TeV, respectively. Other interferences exceeding 1 fb in magnitude were not found.

Based on these results and those in sect. 4 we suggest the following approximative precription for calculating the reaction $e^+e^- \longrightarrow e^+e^- b\bar{b}$. To the incoherently added Higgs signal diagrams, add incoherently the multiperipheral diagrams (second row in Fig. 1), the whole contribution of the single cascade diagrams (third and fourth row in Fig. 1) and the double cascade diagrams with $\gamma^* \to e^+e^-$ and $Z \to b\bar{b}$ decays (fifth row in Fig.1). This approximation is able to describe the complete cross section for reaction (5) with high accuracy (deviations are $\sim 5\%$ or less). Including the non-zero interference terms mentioned above improves the accuracy such that any deviations compared to the complete treatment are reduced to $\sim 1\%$. Since the complete 4-body kinematics is used we expect in principle such an agreement not only for the total cross section but for the event distributions as well. Statistical uncertainties will however dominate the errors for the design luminosities of the colliders considered.

6 Extraction of the Higgs boson signal from background

As already emphasized the number of H^0 events expected in reaction (5) is at least two orders of magnitude smaller than the number of background events. We have already introduced variables (see Figs. 4,5,7,8,9) which indicate that the behaviour of background and H^0 events are so different that appropriate cuts in these variables should allow a clear signal extraction with negligible remaining background.

Fig. 10a (11a) shows the $b\bar{b}$ invariant mass distributions for all events of reaction (5) expected at $\sqrt{s} = 200$ GeV ($\sqrt{s} = 500$ GeV) for an integrated luminosity of $\mathcal{L}$ = 500 pb^{-1} ($\mathcal{L}$ = 10 fb^{-1}). Most of the events are concentrated between $b\bar{b}$-threshold and about $M_{b\bar{b}} = 40$ GeV, independent of $\sqrt{s}$. At 200 GeV, a clear signature for the Higgs boson with $M_{H^0} = 80$ GeV (shown shaded) is prevented by the Z boson tail and additional continuum background. Now, assuming a complete measurement of the final state e^+ and e^- and both quarks, the application of the following cuts

- $|\cos\Theta_b| < 0.94$ and $|\cos\Theta_{\bar{b}}| < 0.94$[1] and $p_\perp^{b\bar{b}} > 45$ GeV and $E_{b\bar{b}} > 90$ GeV
- $|\cos\Theta_{e^-}| < 0.96$ and $|\cos\Theta_{e^+}| < 0.96$ and 60 GeV $< M_{e^+e^-} <$ 110 GeV

results in a clear H^0 signal of 6 events (out of 11) with only one remaining background event (Fig. 10b). If we do not have any e^+ and e^- information (resembling a somewhat more realistic situation since most of the final state

[1]The restriction of the polar angular range for the quarks to $20^0 < \Theta_{b/\bar{b}} < 160^0$ should ensure good measuring capability of the quark fragments.

electrons/positrons remain undetected) and only apply the cuts based on the b and $\bar{b}$ quark information, the resulting $M_{b\bar{b}}$ distribution is presented in Fig. 10c. Beside some remaining Z events, a clear H^0 signal of 7 events remains. Thus, the application of a few simple cuts based on b and $\bar{b}$ quark measurements allows us to extract the Higgs boson almost free of background (provided $M_{H^0} \neq M_{Z^0}$).

At 500 GeV (Fig. 11a) there exists some indication of the H^0 around 140 GeV in the uncutted distribution[2]. The application of the following cuts

- $|cos\Theta_b| < 0.94$ and $|cos\Theta_{\bar{b}}| < 0.94$ and $p_\perp^{b\bar{b}} > 10$ GeV and $E_{b\bar{b}} > 120$ GeV
- $|cos\Theta_{e^-}| < 0.985$ and $|cos\Theta_{e^+}| < 0.985$ and $M_{e^+e^-} > 50$ GeV

results in the distribution shown in Fig. 11b. A clear H^0 signal (shaded histogram) of 54 events (out of 79) is visible over negligible background. The application of less stringent cuts (based again only on the quark information) yields the spectrum in Fig. 11c. Again, the H^0 is clearly seen (75 events of the original signal are retained) and the remaining background is very small.

These results are also of importance for the detection of the H^0 in the reaction $e^+e^- \longrightarrow \nu\bar{\nu}\, b\bar{b}$, since a lot of background comes from reaction (5) with undetected electrons in the final state.

7 Summary and conclusions

A complete tree-level calculation for the reaction $e^+e^- \longrightarrow e^+e^- b\bar{b}$ within the full 4-body kinematics has been carried out at cms energies in the LEPII and NLC regimes. The reaction considered is very interesting from several points of view. It provides a promising possibility for the Higgs boson search, and consequently, together with information from the reactions $e^+e^- \longrightarrow \nu\bar{\nu}\, b\bar{b}$ and $e^+e^- \longrightarrow \mu^+\mu^- b\bar{b}$, it might help to establish the nature of the Higgs boson. Furthermore, reaction (5) represents an important background of Higgs production in the process $e^+e^- \longrightarrow \nu\bar{\nu} b\bar{b}$ and is important for the understanding of several top quark production aspects and in searches for possible new physics at large energies.

We have calculated the total production rate of reaction (5), $e^+e^- \longrightarrow e^+e^- b\bar{b}$, and the expected Higgs cross section between $\sqrt{s} = 200$ GeV and 1 TeV. In general, the H^0 production rate is suppressed by about two orders of magnitude compared with the overall background rate.

[2]This weak H^0 signal is visible by using an enlarged scale for the ordinate.

In order to extract the Higgs signal from such an overwhelming background we have calculated the contributions of different subsets of background diagrams and studied their behaviour in phase space. The results may be summarized as follows. Most of the cross section for the reaction $e^+e^- \longrightarrow e^+e^- b\bar{b}$ comes from the two-photon multiperipheral diagrams (second row in Fig. 1). Next important are contributions from single cascade diagrams (third and forth row in Fig. 1) with off-shell Z production and subsequent $Z \rightarrow b\bar{b}$ decay. Much less important are 2-to-2 body reactions like $e^+e^- \longrightarrow \gamma^* Z$, from which the one with the subsequent decays $\gamma^* \rightarrow e^+e^-$ and $Z \rightarrow b\bar{b}$ is found to be the dominant one. Double Z production is comparable to the Higgs production rate. Contributions by the s-channel diagrams (last row in Fig. 1) are very small and can be neglected in the energy range studied. We have searched for significant interferences between the diagrams contributing to reaction (5). They all were found to be negligible (smaller than 1 fb in magnitude) except those between single cascade diagrams with $Z \rightarrow b\bar{b}$ and double cascade diagrams with $\gamma^* \rightarrow e^+e^-$ and $Z \rightarrow b\bar{b}$ decays, and between single cascade diagrams with $\gamma^* \rightarrow e^+e^-$ and $Z \rightarrow b\bar{b}$ themselve. Based on these results a simple approximative description for reaction (5) is suggested which might be useful for future event generators incorporating the complete 4-body kinematics.

Concerning the extraction of the Higgs signal we have demonstrated that by the application of few simple cuts based only on b and $\bar{b}$ quark information the overwhelming background can be reduced to a negligible level while retaining most of the H^0 events. Encouraging results were obtained even in the case of only a few H^0 events expected in the presence of two orders of magnitude higher background (as in the LEPII energy range).

We are aware that a thorough study would have to include electroweak and QCD corrections as well as a realistic detector simulation. The aim of this paper was, however, to study the contributions of the different subsets of diagrams (partially omitted so far in related investigations), their interference pattern and the impact on the detection probability of the Higgs boson.

A Appendix

1. A simple estimation for the multiperipheral diagram cross section is obtained by means of the (improved) Weizsäcker-Williams approximation (WWA) [22, 23]. The total cross section reads

$$\sigma = \int_{x_{min}}^{x_{max}} dx_1 dx_2 \Theta(\hat{s} - 4m_b^2) \hat{\sigma}(\gamma\gamma \rightarrow b\bar{b}) f_\gamma(x_1, \delta) f_\gamma(x_2, \delta) \qquad \text{(A-1)}$$

with

$$f(x,\delta) = \frac{\alpha}{2\pi}\left[\frac{1+(1-x)^2}{x}\log\frac{1-x}{x^2\delta} - 2\frac{1-x-x^2\delta}{x}\right]. \qquad \text{(A-2)}$$

x is the fractional energy transfered by the photon, with $x_{min} = 4m_b^2/s$, $x_{max} = 1$ and $\delta = m_e^2/4m_b^2$, and

$$\hat{\sigma}(\gamma\gamma \to b\bar{b}) = \frac{22\alpha^2\pi}{27\hat{s}}\left\{(3-\beta^4)ln\frac{1+\beta}{1-\beta} - 2\beta(2-\beta^2)\right\}, \qquad \text{(A-3)}$$

the cross section for $b\bar{b}$ pair production in $\gamma\gamma$ collision [24], with

$$\beta = \sqrt{1-4\frac{m_b^2}{\hat{s}}} \qquad \text{and} \qquad \hat{s} = x_1x_2s. \qquad \text{(A-4)}$$

The numerical results using formula (A-1) are presented in Fig. 6 as dashed curve.

2. For the semi-analytical approximations of the single and double cascade contributions we start from general formulas for either e^+e^- or γe interactions with one or two off-shell photons produced in association with n particles and subsequent decay(s) $\gamma^* \to f\bar{f}$:

$$\sigma(e^+e^-(\gamma e) \to 1 + ... + n + \gamma^*(\to f\bar{f}) \simeq \qquad \text{(A-5)}$$

$$\frac{1}{\pi}\int_{4m_f^2}^{(\sqrt{s}-\tilde{m})^2}\frac{dM_\gamma^2}{M_\gamma^3}\hat{\sigma}(e^+e^-(\gamma e) \to 1 + ... + n + \gamma^*)\Gamma(\gamma^* \to f\bar{f})$$

and

$$\sigma(e^+e^-(\gamma e) \to 1 + ... + n + \gamma_1^*(\to f_1\bar{f}_1)\gamma_2^*(\to f_2\bar{f}_2) \simeq \qquad \text{(A-6)}$$

$$\frac{1}{\pi^2}\int_{4m_{f_1}^2}^{(\sqrt{s}-\tilde{m}-2m_{f_2})^2}\frac{dM_{\gamma_1^2}}{M_{\gamma_1^2}}\int_{4m_{f_2}^2}^{(\sqrt{s}-\tilde{m}-M_{\gamma_1})^2}\frac{dM_{\gamma_2^2}}{M_{\gamma_2^2}} *$$

$$*\hat{\sigma}(e^+e^-(\gamma e) \to 1 + ... + n + \gamma_1^*\gamma_1^*)\Gamma(\gamma_1^* \to f_1\bar{f}_1)\Gamma(\gamma_2^* \to f_2\bar{f}_2)$$

with $\tilde{m} = \sum_{i=1}^n m_i$ and the off-shell photon decay width

$$\Gamma(\gamma^* \to f\bar{f}) = \frac{\alpha}{3}Q_f^2T_cM_\gamma(1+2x_f)\sqrt{1-4x_f}, \qquad \text{(A-7)}$$

where $x_f = m_f^2/M_\gamma^2$, $Q_f^2 = 1/9$ for the b-quark and 1 for the electron. The color factor T_c is 3 for b-quarks and 1 for electrons.

Selecting now from all single cascade diagrams in Fig. 1 only those with photon exchange in the t-channel and Z boson production with subsequent $Z \to b\bar{b}$ decay we obtain for the cross section

$$\sigma_Z = \int_{x_{min}}^{x_{max}}dx\int_{Q^2_{min}}^{Q^2_{max}}dQ^2f_\gamma(x,Q^2)\hat{\sigma}(\gamma^*e \to Ze;Q^2)Br(Z \to b\bar{b}) \qquad \text{(A-8)}$$

in the narrow width approximation for Z bosons. The singular behaviour of the $\gamma^*e \to Ze$ cross section requires to consider virtual initial state photons with -Q^2 [25].

For the effective photon spectrum within the electron we use the (improved) Weizsäcker-Williams approximation [22, 23] before the integration over Q^2

$$f_\gamma(x,Q^2) = \frac{\alpha}{2\pi}\left[\frac{1+(1-x)^2}{xQ^2} - 2m_e^2x\frac{1}{Q^4}\right] \qquad \text{(A-9)}$$

with the following integration limits:

$$\begin{aligned} Q^2_{min} &= m_e^2\frac{x^2}{1-x}; & Q^2_{max} &= M_Z^2; \\ x_{min} &= \frac{(M_Z+m_e)^2}{s}; & x_{max} &= \frac{(\sqrt{s}-m_e)^2}{s}. \end{aligned} \qquad \text{(A-10)}$$

The cross section for the subprocess $\gamma^*e \to Be$, where B means either the Z boson or a γ^*, can be written as

$$\hat{\sigma}(\gamma^*e \to Be;Q^2) = \frac{\alpha^2\pi}{\hat{s}}C_B\left\{2(1-2x_B+2x_B^2)\ln\frac{\alpha+\beta}{\alpha-\beta} + \right. \qquad \text{(A-11)}$$

$$\left.\beta\frac{x_e(1+7x_B)+x_\gamma x_B(1-2x_B+3x_B^2)}{x_e-x_\gamma x_B(1-x_B)} + \mathcal{O}(x_e,x_\gamma)\right\}$$

with $x_Z = M_Z^2/\hat{s}$ or $x_{\gamma_f^*} = M_{\gamma_f^*}/\hat{s}$,

$$C_Z = \frac{1-4s_W^2+8s_W^4}{12s_W^2c_W^2} \quad \text{or} \quad C_{\gamma_f^*} = \frac{2}{3},$$

$$\alpha = 1 - x_B + x_ex_B - x_e^2 - x_\gamma(1-x_B-x_e),$$

$$\beta = [(1+(x_e-x_\gamma)^2-2x_e-2x_\gamma)(1+(x_e-x_B)^2-2x_e-2x_B)]^{1/2},$$

$$x_e = \frac{m_e^2}{\hat{s}}, \qquad x_\gamma = -\frac{Q_\gamma^2}{\hat{s}}, \qquad \hat{s} = xs$$

and s_W denotes the sinus of the Weinberg angle. The application of formula (A-11) for the case $B = Z$ yields, after multiplication with 2 due to photon emission either by the initial state electron or positron, only one part of the relevant cross section. The remaining part comes from subprocess $\gamma^* e \to \gamma^* e$, i.e. for $B = \gamma^*$. Its general cross section can be estimated using formula (A-5) and the WWA [22, 23] as

$$\sigma_{\gamma^*} = \int_{x_{min}}^{x_{max}} dx \int_{Q^2_{min}}^{Q^2_{max}} dQ^2 \frac{1}{\pi} \int \frac{dM^2}{M^3} f_\gamma(x,Q^2) \hat{\sigma}(\gamma^* e \to \gamma^* e; Q^2) \Gamma(\gamma^* \to b\bar{b}) \tag{A-12}$$

where $\hat{\sigma}$ is given by (A-11). The integration limits in (A-12) are obtained using $2m_b$ instad of M_Z in (A-10).

The sum of the cross sections (A-8) and (A-12) are shown in Fig. 6 as dashed curve. They represent that part of the single cascade cross section which only occurs via t-channel photon exchanges.

3. The double cascade contribution might be divided into three subreactions, $e^+e^- \longrightarrow \gamma^*\gamma^*$, $e^+e^- \longrightarrow \gamma^* Z$ and $e^+e^- \longrightarrow ZZ$, with subsequent Z and γ^* decays to the final state $e^+e^-\, b\bar{b}$. The cross section for the first reaction, $e^+e^- \longrightarrow \gamma^*\gamma^*$, is obtained from eq. (A-6) and formulas of refs. [26, 27] which might be summarized as follows

$$\hat{\sigma}(e^+e^- \to Z/\gamma^*, Z/\gamma^*) = \frac{\alpha^2\pi}{s} C_D \{\ln\frac{\alpha_D+\beta_D}{\alpha_D-\beta_D} A_D - 3\beta_D\alpha_D\} \tag{A-13}$$

with

$$C_D = \frac{4}{1-x_1-x_2}, \qquad \alpha_D = 1-x_1-x_2,$$

$$\beta_D = \sqrt{1+(x_1-x_2)^2-2x_1-2x_2}, \qquad A_D = 1+(x_1+x_2)^2,$$

$$x_1 = M^2_{\gamma_1^*}/s, \qquad \text{and} \qquad \mathrm{x_2 = M^2_{\gamma_2^*}/s.}$$

The results of this approach are shown as dashed curve in Fig. 6.

For the reaction $e^+e^- \longrightarrow \gamma^* Z$ we start from eqn. (A-5) using the expression (A-13) with

$$\begin{aligned} C_D &= \frac{1-4s_W^2+8s_W^4}{2c_W^2 s_W^2}\frac{1}{1-x_{\gamma_f^*}-x_Z}; \\ \alpha_D &= 1-x_Z-x_{\gamma_f^*}; \\ \beta_D &= \sqrt{1+(x_Z-x_{\gamma_f^*})^2-2x_Z-2x_{\gamma_f^*}} \\ A_D &= 1+(x_Z^2+x_{\gamma_f^*})^2, \\ x_{\gamma^*} &= \frac{M^2_{\gamma^*}}{s} \end{aligned}$$

and the narrow width approximation of the Z boson, i.e. multiplying the resulting cross section with the appropriate branching ratio $Br(Z \to b\bar{b}\,)$, respectively, $Br(Z \to e^+e^-\,)$. The results of this procedure are shown as dashed curve in Fig. 6 for the two possiblilities $e^+e^- \longrightarrow \gamma^* Z \to (e^+e^-\,)(b\bar{b}\,)$ and $e^+e^- \longrightarrow \gamma^* Z \to (b\bar{b}\,)(e^+e^-\,)$.

The cross section for the reaction $e^+e^- \longrightarrow ZZ \to (e^+e^-\,)(b\bar{b}\,)$ is obtained from eqn. (A-13) and the narrow width approximation for the Z bosons with

$$C_D = \frac{1-s_W^2+24s_W^4-32s_W^6+38s_W^8}{16c_W^4 s_W^4}\frac{1}{1-2x_Z},$$

$$\alpha_D = 1-2x_Z, \qquad \beta_D = \sqrt{1-4x_Z},$$

$$A_D = 1+4x_Z^2 \qquad \text{and} \qquad \mathrm{x_Z = \frac{M_Z^2}{s}}.$$

The results of this approximation are shown as dashed curve in Fig. 6.

Acknowledgements

We would like to thank I. Ginzburg for useful discussions and V. Ilyin and A. Pukhov for discussions and the help with CompHEP calculations. E.B. and S. Sh. are grateful to P. Söding for his interest and support, and to DESY-IfH Zeuthen for the kind hospitality. The work has partially been supported by the ISF grant No. M9B000 and by the INTAS grant INTAS-93-1180.

References

[1] S. L. Glashow, Nucl. Phys. **22** (1961) 579;
S. Weinberg, Phys. Rev. Lett. **19** (1967) 1264;
A. Salam, Elementary Particle Theory, ed. by N. Svartholm, Stockholm (1968), 367.

[2] J. F. Gunion, H. E. Haber, G. Kane and S. Dawson, The Higgs Hunter's Guide, Addison-Wesley 1990;

[3] H. E. Haber, in Physics and Experiments with Linear Colliders, ed. by R. Orava, P. Eerola and M. Nordberg, World Scientific Publishing Co.,1992,p. 235.

[4] A. Djouadi, D. Haidt and P. M. Zerwas, Proc. of the Workshop - Munich, Annecy, Hamburg, 1991, ed. by P. M. Zerwas, DESY Report 92-123A, p. 1;
A Djouadi, D. Haidt, B. A. Kniehl, B. Mele and P. M. Zerwas, Proc. of the Workshop - Munich, Annecy, Hamburg, 1991, ed. by P. M. Zerwas, DESY Report 92-123A, p. 11.

[5] P. Janot, LAL preprint 93-38 (July 1993), talk given at the Second Int. Workshop on Physics and Experiments with Linear e^+e^- Collider, Waikoloa, Hawaii, 1993.

[6] V. Barger, K. Cheung, A. Djouadi, B.A. Kniehl and P. M. Zerwas, Phys. Rev. **D49** (1994) 79.

[7] E. Boos, M. Sachwitz, H.J. Schreiber and S. Shichanin, Z. Phys. C61, (1994) 675.

[8] E. Boos, M. Sachwitz, H.J. Schreiber and S. Shichanin, preprint DESY 93-183.

[9] M. Dubinin, V. Edneral, Y. Kurihara and Y. Shimizu, KEK Preprint 93-138 (1993), submitted to Phys. Lett. B.

[10] E. E. Boos et al. Proc. of the XXVIth Recontre de Moriond, ed. by J. Tran Than Van, Edition Frontiers, 1991, p. 501;
E. E. Boos et al., Proc. of the Second Int. Workshop on Software Engineering, ed. by D. Perred-Gallix, World Scientific, 1992, p. 665;
E. E. Boos et al., KEK preprint 92-47, 1992.

[11] S. Kawabata, Comp. Phys. Commun. **41** (1986) 127.

[12] F.A. Berends, P.H. Daverveldt and R. Kleiss, Phys. Lett. **B148** (1984) 489.

[13] F.A. Berends, P.H. Daverveldt and R. Kleiss, Nucl. Phys. **B253** (1985) 441.

[14] J.A.M. Vermaseren, Nucl. Phys. **B229** (1983) 347.

[15] J. Hilgart, R. Kleiss and F. Le Diberder, Comp. Phys. Commun. **75** (1993) 191.

[16] E. Boos et al., Phys. Lett. **B326** (1994) 190.

[17] K. Hagiwara, H. Iwasaki, A. Miyamoto and D. Zeppenfeld, Nucl. Phys. **B365** (1991) 544.

[18] V. Barger, K. Cheung, B.A. Kniehl and R. Phillips, Phys. Rev. **D46** (1992) 3752.

[19] L. Landau and E. Lifshitz, Sov. Phys. 5 (1934) 206.

[20] G. Burgers, Proc. of the Workshop on Physics at Future Accelerators, La Thuile and Geneva (1987), CERN 87-07 Vol. II, p. 360.

[21] E.A. Kuraev and L.N. Lipatov, Sov. J. Nucl. Phys. **16** (1973)584.

[22] C. F. Weizsäcker, Z. Phys. **88** (1934) 612;
E. J. Williams, Phys. Rev. **45** (1934) 729.

[23] S. Frixone, M.L. Mangano, P. Nason and G. Ridolfi, preprint CERN-TH. 7032/93.

[24] T. L. Barklow, preprint SLAC-PUB-5364(1990).

[25] D.P. Sushkov, V.V. Flambaum and I.B. Khriplovich, Sov. J. Nucl. Phys. **20** (1975) 537.

[26] E. Eichten, I. Hinchliffe, K,D. Lane and C. Quigg, Rev. Mod. Phys. **56** (1984) 579.

[27] E.L. Berger, E. Braaten and R.D. Field, Nucl. Phys. **B239** (1984) 52.

Table Caption

Table 1: Number of H^0 events expected for an integrated luminosity of 500 pb^{-1} and 10 fb^{-1} at 200 GeV and 500 GeV, respectively, for five Higgs masses.

Figure Caption

Fig. 1: Lowest order Feynman diagrams contributing to the reaction $e^+e^- \longrightarrow e^+e^- b\bar{b}$.

Fig. 2: Cross sections for the reaction $e^+e^- \longrightarrow e^+e^- b\bar{b}$ and the H^0 cross section as functions of the cms energy $\sqrt{s}$.

Fig. 3: H^0 production cross section in the reaction $e^+e^- \longrightarrow e^+e^- b\bar{b}$. Fig. 3a represents the total cross section, Fig. 3b the cross section expected from the Higgsstrahlung mechanism, Fig. 3c the cross section expected from the fusion mechanism and Fig. 3d the interference between both mechanisms.

Fig. 4: Differential distributions for H^0 events expected for $M_{H^0} = 80$ GeV and an integrated luminosity of $\mathcal{L} = 500$ pb^{-1} at $\sqrt{s} = 200$ GeV.

Fig. 5: Differential distributions for H^0 events expected for $M_{H^0} = 140$ GeV and an integrated luminosity of $\mathcal{L} = 10$ fb^{-1} at $\sqrt{s} = 500$ GeV.

Fig. 6: Cross sections for different background contributions as functions of the cms energy $\sqrt{s}$. The full curves correspond to the complete calculations whereas the dashed curves were obtained from simple approximations as presented in the Appendix.

Fig. 7: Multiperipheral background events as functions of the cosine of the e^- production angle, cos Θ_{e^-}, the total $b\bar{b}$ transverse momentum, $p_\perp^{b\bar{b}}$, the total $b\bar{b}$ energy, $\mathrm{E}_{b\bar{b}}$, as expected for $\sqrt{s} = 200$ GeV ($\sqrt{s} = 500$ GeV) and an integrated luminosity of 500 pb^{-1} (10 fb^{-1}).

Fig. 8: Single cascade background events as functions of the cosine of the e^- production angle, cos Θ_{e^-}, the total $b\bar{b}$ transverse momentum, $p_\perp^{b\bar{b}}$, the total $b\bar{b}$ energy, $\mathrm{E}_{b\bar{b}}$, as expected for $\sqrt{s} = 200$ GeV ($\sqrt{s} = 500$ GeV) and an integrated luminosity of 500 pb^{-1} (10 fb^{-1}).

Fig. 9: Double cascade background events as functions of the cosine of the e^- production angle, cos Θ_{e^-}, the total $b\bar{b}$ transverse momentum, $p_\perp^{b\bar{b}}$, the total $b\bar{b}$ energy, $\mathrm{E}_{b\bar{b}}$, as expected for $\sqrt{s} = 200$ GeV ($\sqrt{s} = 500$ GeV) and an integrated luminosity of 500 pb^{-1} (10 fb^{-1}).

Fig. 10: Number of events of reaction (5) as function of the $b\bar{b}$ invariant mass at $\sqrt{s} = 200$ GeV for an integrated luminosity of 500 pb^{-1}. Fig. 10a shows the distribution without cuts, Fig. 10b results after the application of all cuts (see text) and Fig. 10c is obtained after applying only cuts based on $b/\bar{b}$ quark information. The H^0 events are shown as hatched histograms.

Fig. 11: Number of events of reaction (5) as function of the $b\bar{b}$ invariant mass at $\sqrt{s} = 500$ GeV for an integrated luminosity of 10 fb^{-1}. Fig. 10a shows the distribution without cuts, Fig. 10b results after the application of all cuts (see text) and Fig. 10c is obtained after applying only cuts based on $b/\bar{b}$ quark information. The H^0 events are shown as hatched histograms.

M_{H^0} (GeV) \ $\sqrt{s}$	200 GeV	500 GeV
80	11	124
M_Z	8	114
100	5	104
120	-	94
140	-	79

Table 1:

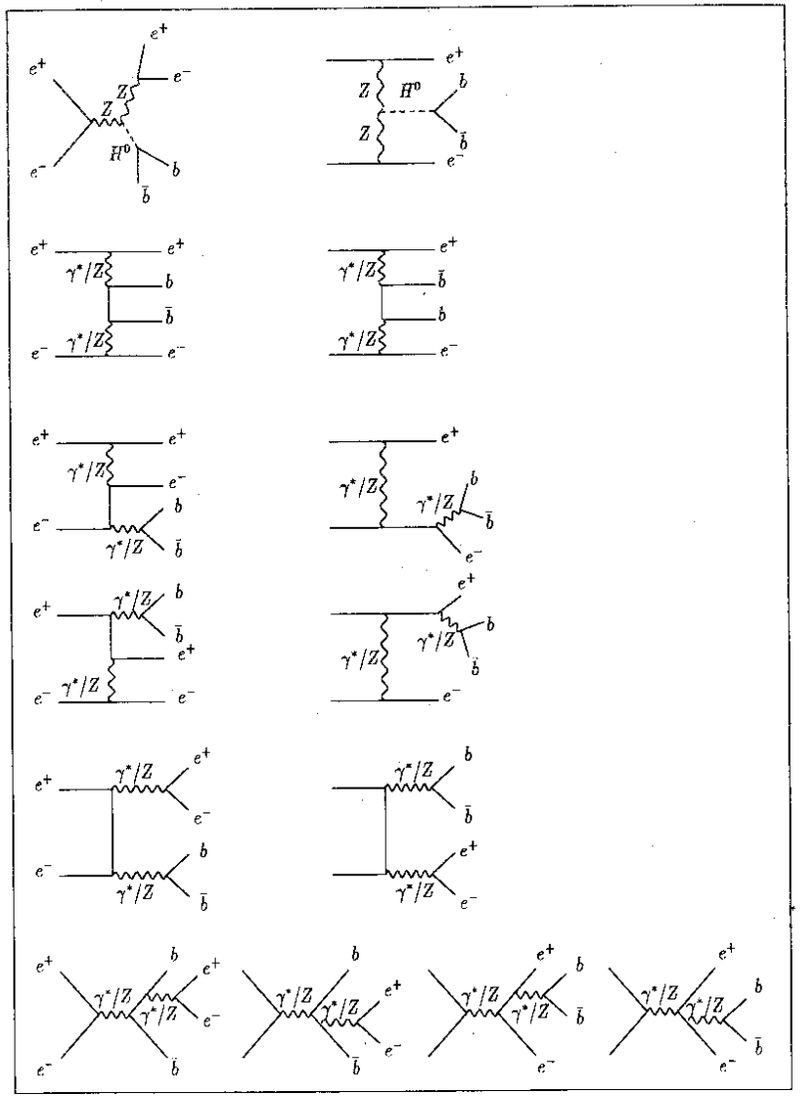

Figure 1:

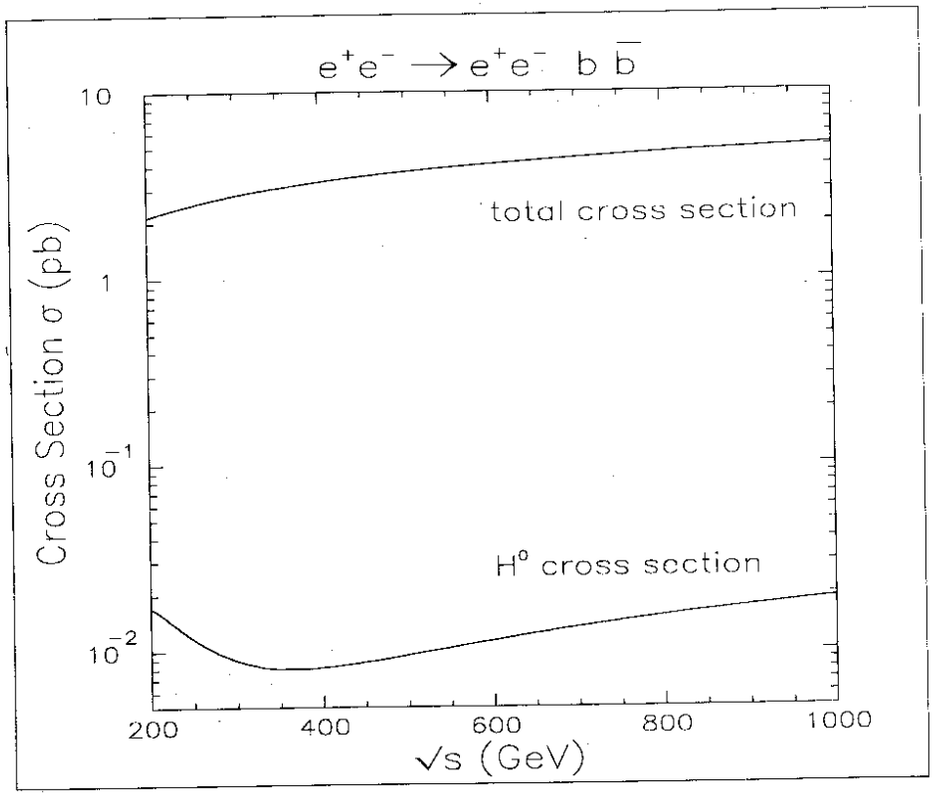

Figure 2:

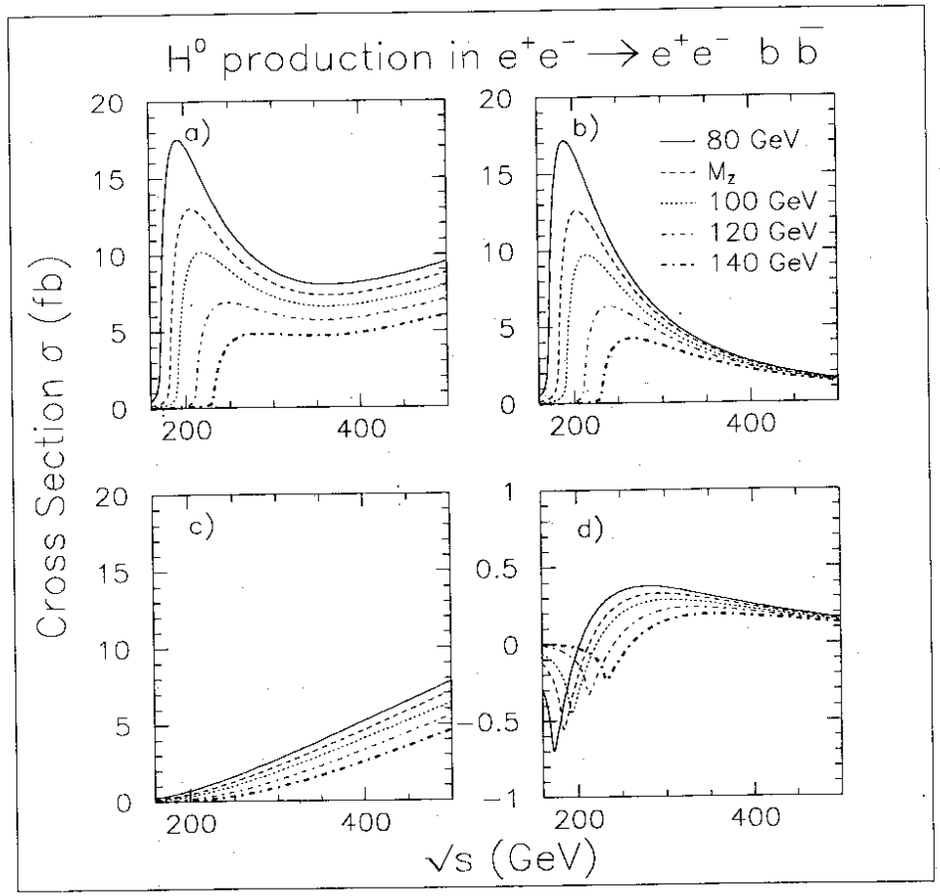

Figure 3:

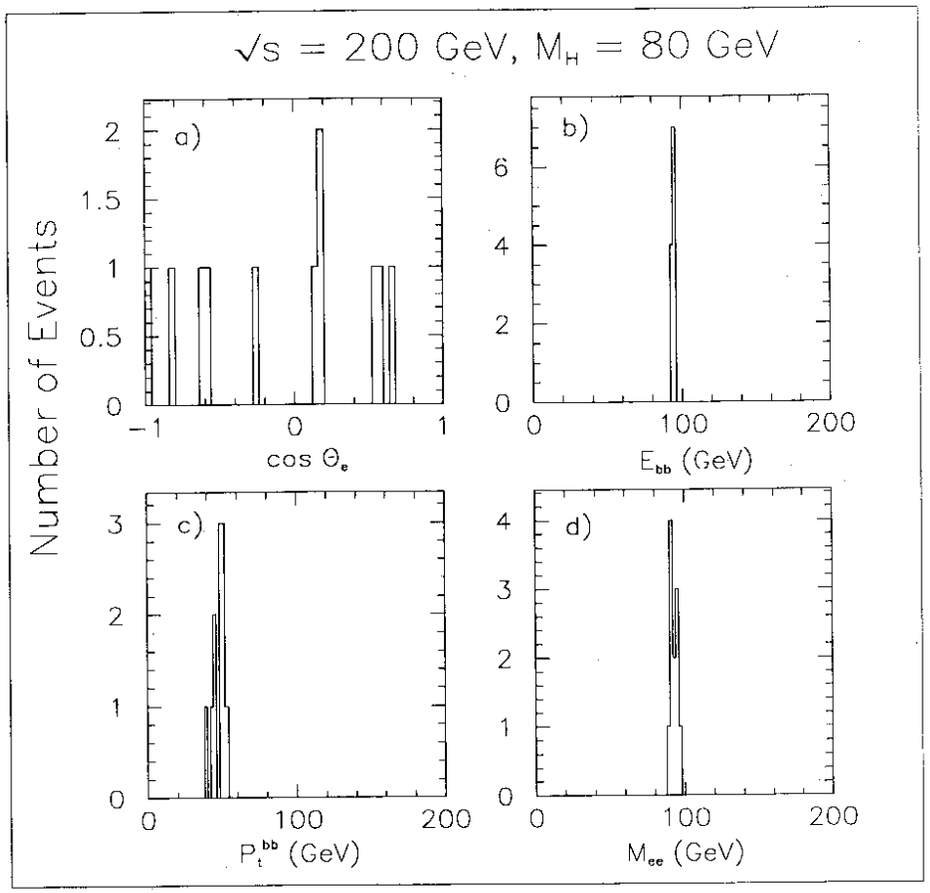

Figure 4:

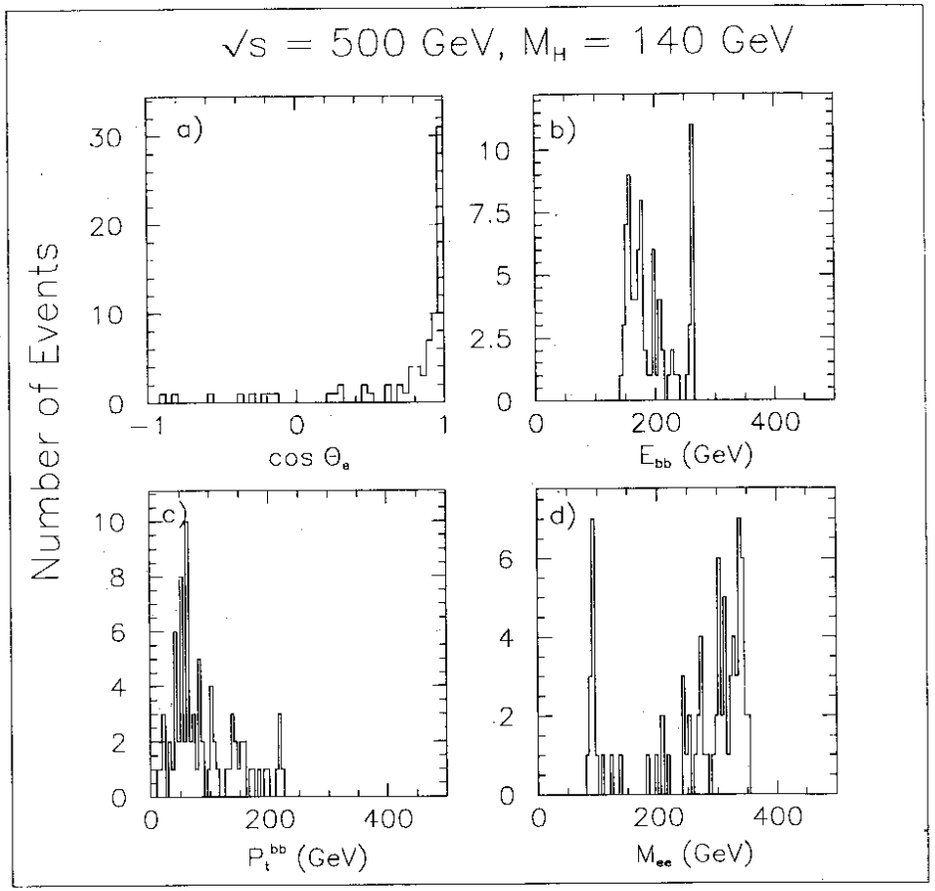

Figure 5:

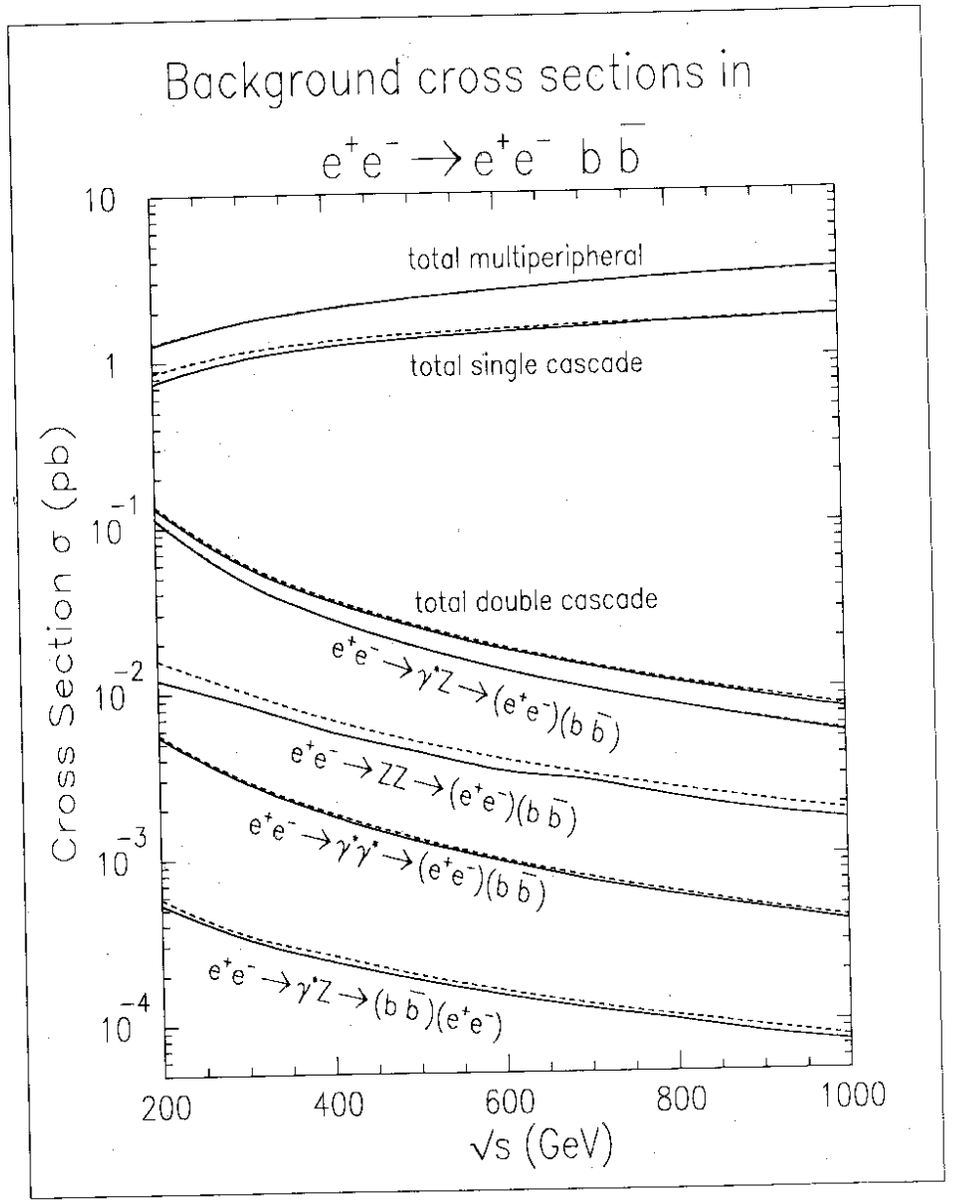

Figure 6:

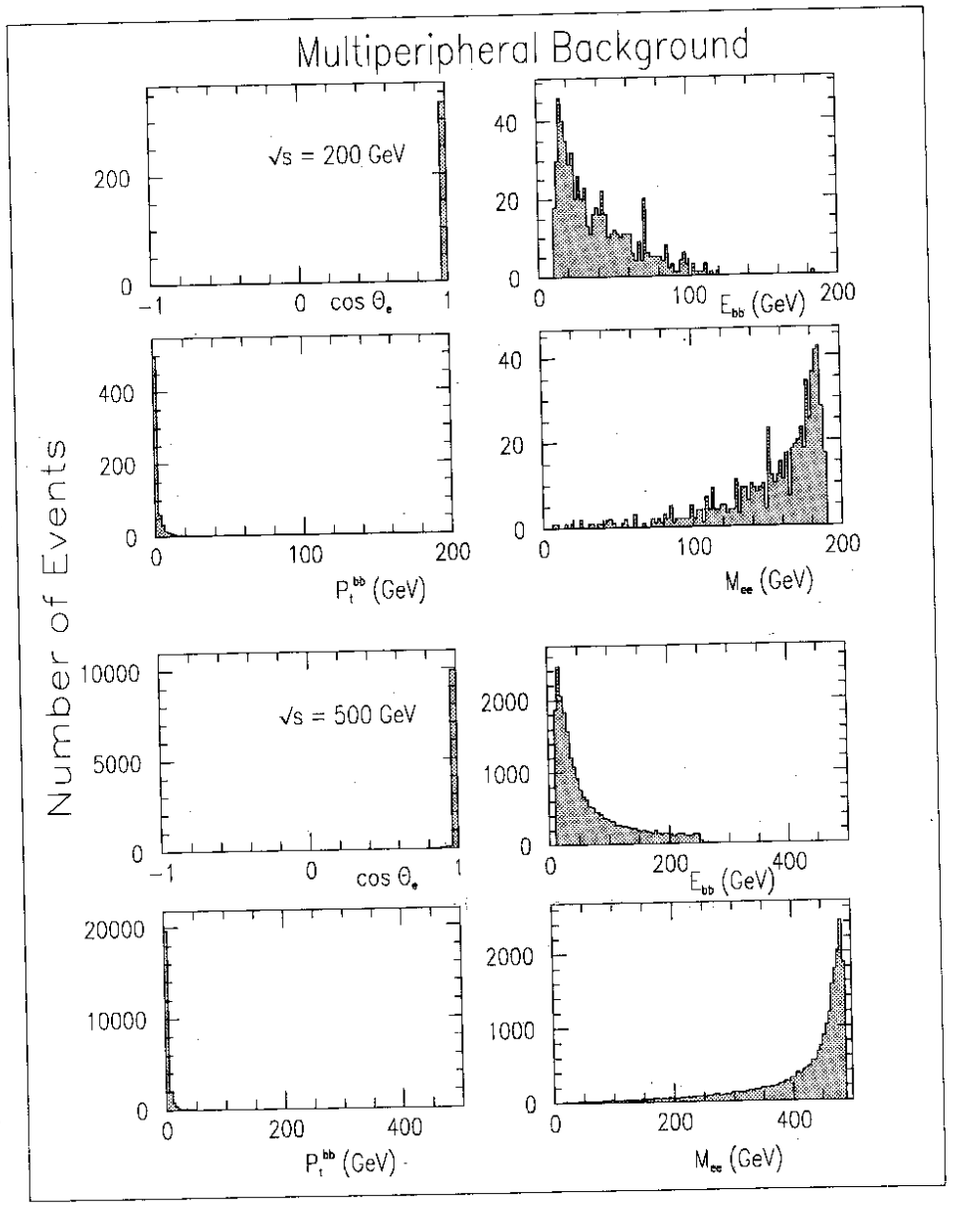

Figure 7:

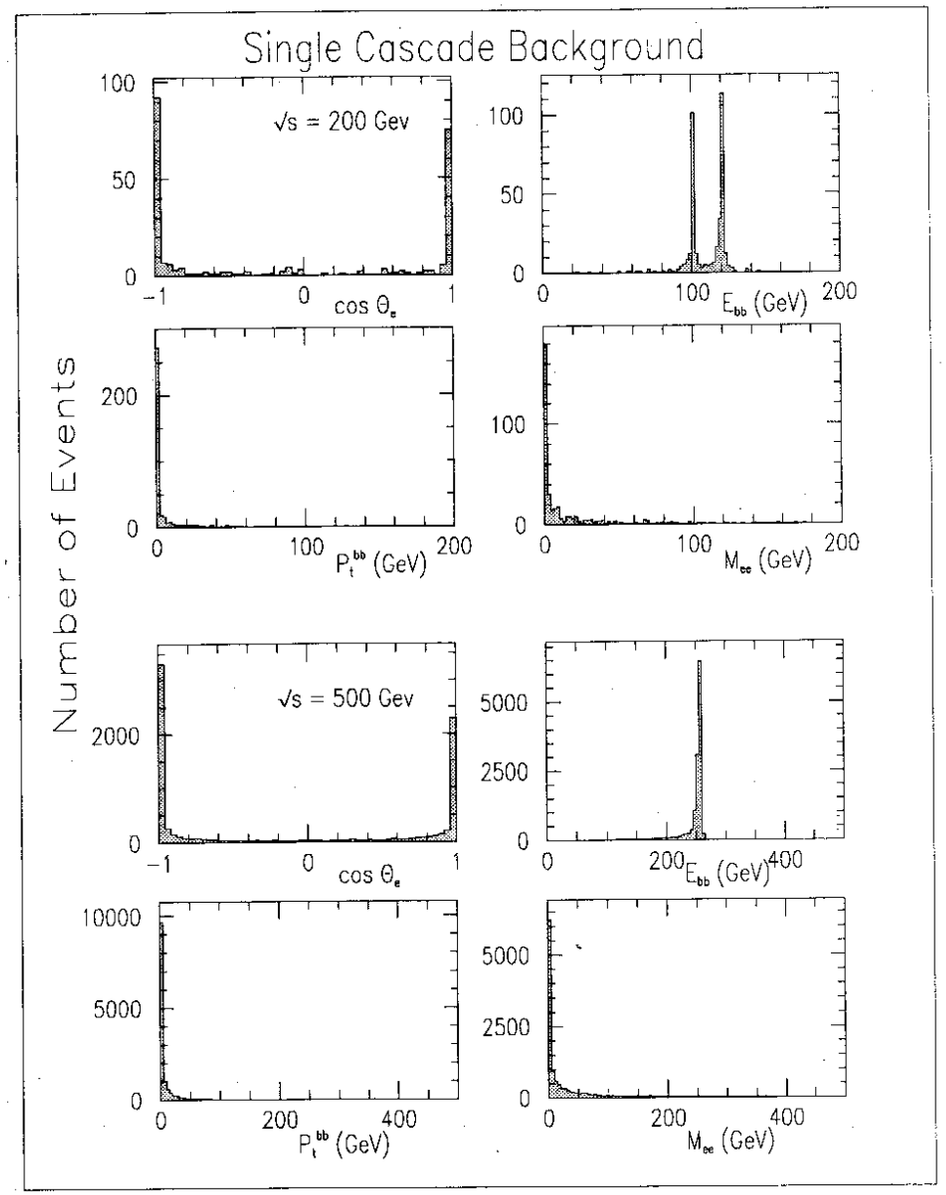

Figure 8:

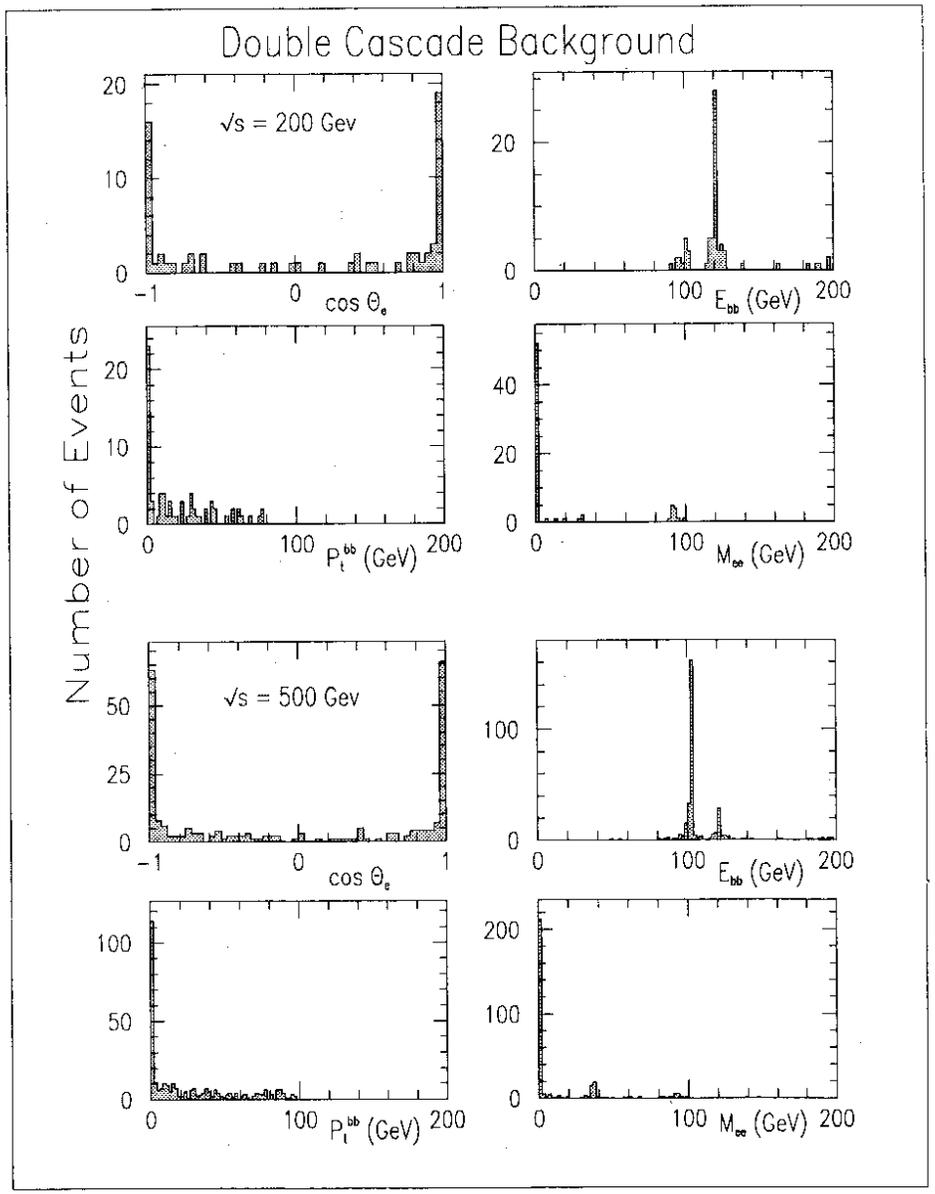

Figure 9:

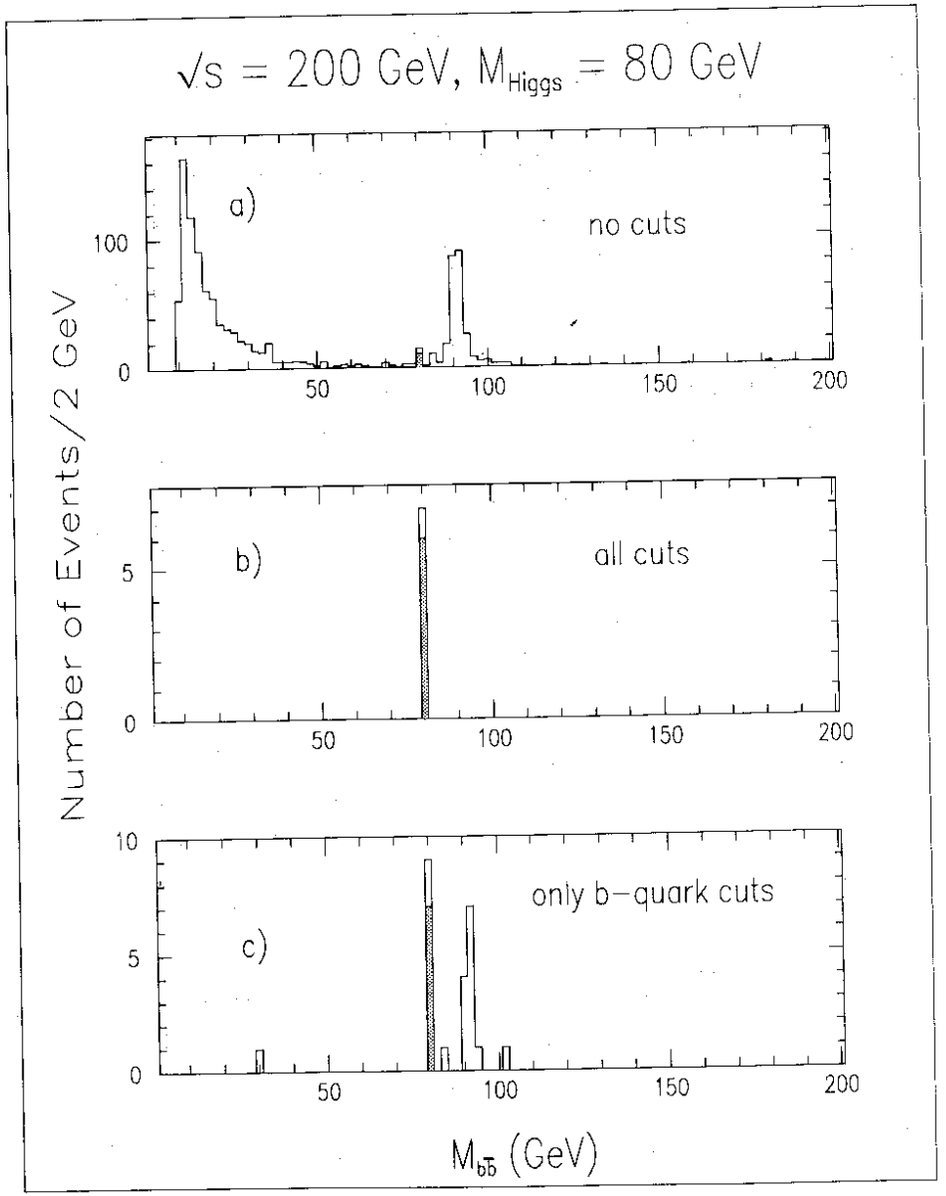

Figure 10:

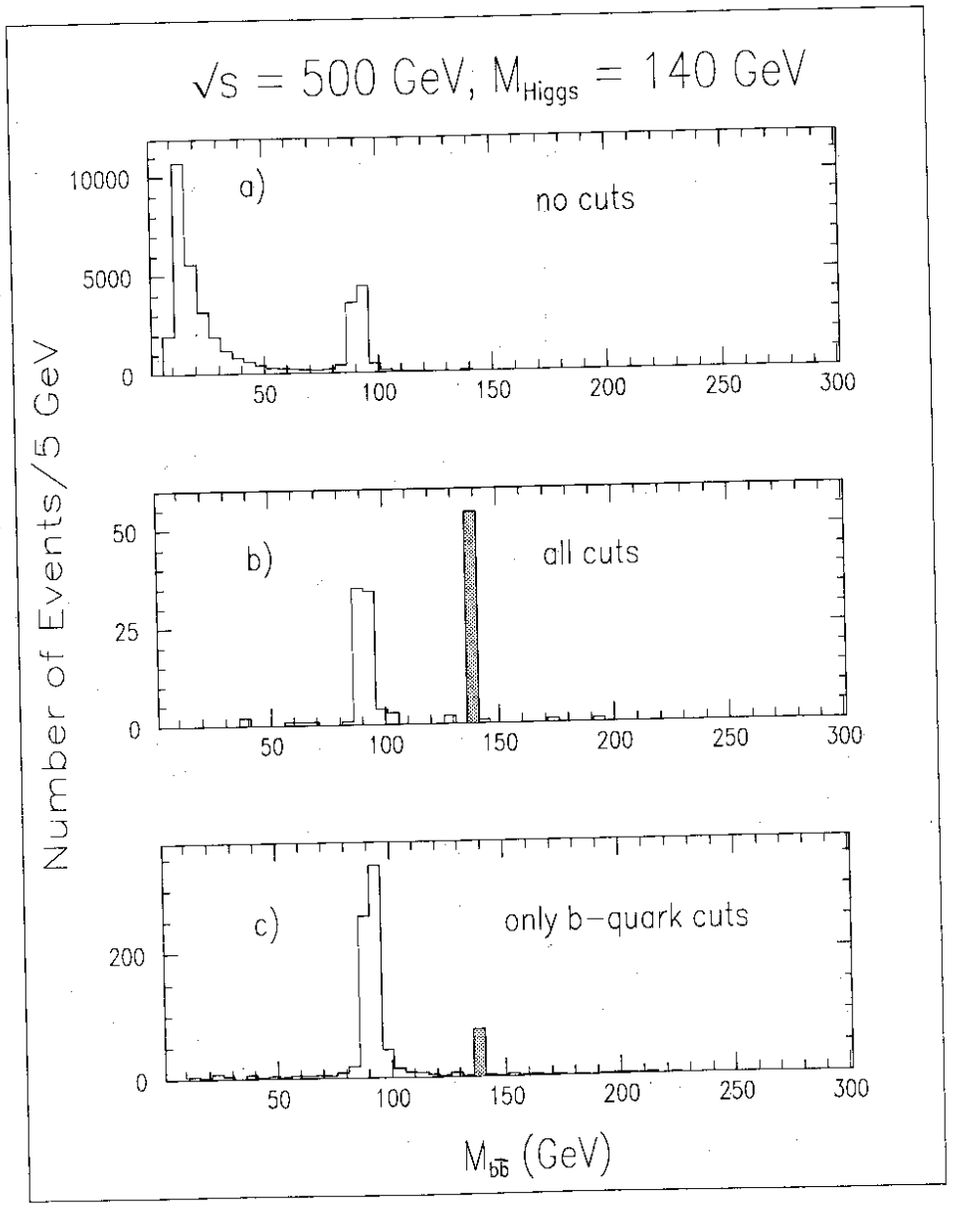

Figure 11: